IMPROVED THERMOMETER FOR HIGH-RESOLUTION AIRBORNE MEASUREMENTS

Wojciech Kumala[1], Paweł Klimczewski[2], Szymon P. Malinowski[1],
Kamil Kwiatkowski[1], Karol Wędołowski[2], Jacek Kopeć[1]

[1]University of Warsaw, Faculty of Physics, Institute of Geophysics, Pasteura 7, 02-093 Warsaw, Poland
[2]University of Warsaw, Faculty of Physics, Institute of Theoretical Physics, Hoża 69, 00-681 Warsaw, Poland

1.INTRODUCTION

A prototype miniature thermometer UFT-2 was developed from the former Ultra Fast Thermometer UFT(Haman et al., 1997, 2001). It is aimed at very high resolution airborne measurements in clear air as well as in clouds. The sensing element is an ultra-thin resistive wire (1.25 µm in diameter). Tests with alternative, more robust, thin film resistive sensor are on the way. The sensing element is placed behind a 0.25mm thick and 4mm long rod that protects it from cloud droplets and ice crystals. The whole thermometer has no moving parts, is thinner than a pencil, and potentially may be integrated with cloud droplet sensors like FFSSP or CDP. Miniaturization of the sensor results in lower flow distortions and reduced aerodynamic noise compared to previous UFT thermometers . This improvement was confirmed both in preliminary test flights and in numerical simulations of the airflow around the sensor head. Frequency response of UFT-2 reaches 10kHz in flight conditions, corresponding to ~2mm spatial resolution. In order to collect data from such a fast sensor, a small autonomous acquisition system (DAS) recording on a memory flash card up to 200000 of 16-bit samples per second was built. UFT-2 together with dedicated DAS form small, battery powered package which can be easily adopted on various aircraft, including UAS. To fully characterize the prototype UFT-2 more tests with different sensing elements and under various atmospheric and flight conditions are needed.

2. DESIGN

A significant modification of the UFT geometry was introduced, in order to avoid moving parts which are difficult to certify on a research aircraft. Rotatable anti-droplet shield was replaced by a fixed protecting rod. Studies of the airflow around fixed anti droplet shield lead to the conclusion that the fixed sensor should be smaller: the Reynolds number Re of the flow behind the rod had to be reduced to diminish wake effects.

The new sensor is 34mm long and 4mm wide. The anti-droplet protecting rod has a diameter of 0.25mm and is placed 0.75mm in front of the sensing element. Such geometry, should ensure satisfactory protection of the sensing element from wetting by cloud droplets and hitting by ice crystals. At the typical airspeed of 100m/s flow around the rod is characterized by Re~1600 (Re~800 at 50m/s). At this values of Re pressure fluctuations (and consequently temperature fluctuations) in the vortices shedding from the rod are reduced.

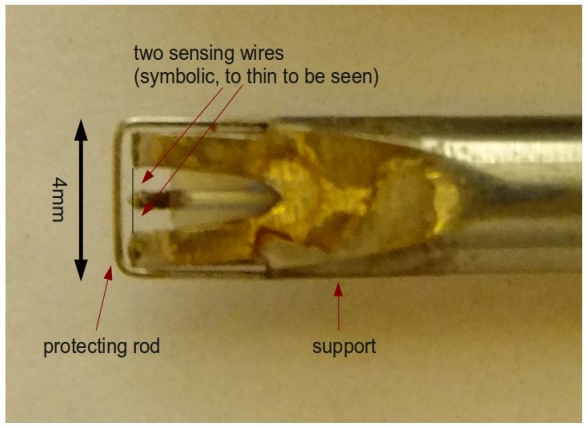

***Fig.1**. Prototype UFT-II – sensor head.*

As in former UFT's, the sensor is a thermoresistive thin and long cylinder. It is spanned between the central core coaxial cable connector and external supports. Symmetric collection of the signal prevents external electromagnetic interferences. A photograph of the prototype of the new UFT-2 with no moving part is presented in Fig.1.

3. MANUFACTURING

After a series of laboratory tests of various materials and assembly techniques, a following construction of the sensor was chosen:

- sensor shell, 34mm long, made of stainless steel (AISI 304) tube of external diameter of 4mm with 1.6mm duct for isolated central conductor;

- coaxial cable (Habia flexiform 405 FJ) to collect signal from the sensing element;

- protecting rod of stainless steel (AISI 321), 0.25mm in diameter, located 0.75mm in front of sensing resistive wires;

- sensing platinum wires,1.25μm in diameter, or metalized glass fibers 5μm in diameter;

A Wollaston technique is adopted to apply fine wires as sensing elements. Wollaston wire: 25μm thick silver shell with the inner platinum core 1.25μm in diameter, is soldered with Au80/Sn20 alloy to the supports. After soldering it is etched in 60% nitric acid in order to remove silver shell.

In alternative version a 5μm thick fiberglass cylinder of is soldered with indium to the support. Then it is metalized with gold using Quorum Technologies Q150R sputter coater to achieve resistance of about 50Ω at 20°C (Fig.2).

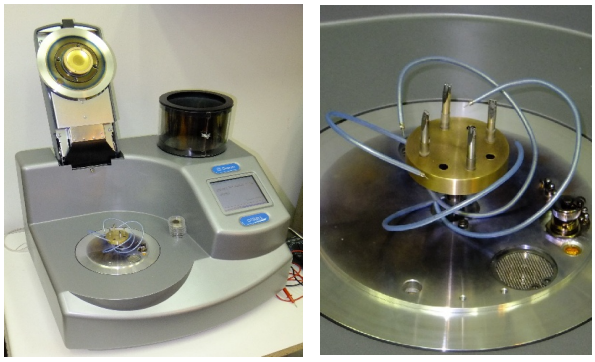

***Fig.2**. Four UFT-2 senors ready for coating with gold in a special clamp in sputter coater.*

A series of 10 prototype UFT-2 sensors was built for the laboratory and flight tests. These sensors are prepared to work with a modified (changed resistors) bridge/amplifier system originating at UFT-M thermometers.

UFT-2 sensors' stability and linearity were tested in laboratory. In course of tests readings from UFT-2 sensors in thermally stable environment were compared to standard PT-100 thermometer.

Laboratory tested specifications of the new UFT-2 with the dedicated data acquisition system are the following:

- temperature dependence: 0.15Ω/K
- sensitivity : 21mV/K

Due to differences between the sensors resulting from manufacturing, sensitivities of individual sensors may differ from this value by less than 10%.

Selected sensors were tested in a laminar wind tunnel at the airspeeds up to 40m/s. No significant effects of vortex shedding was observed, but it occurred that platinum sensing wires are very delicate and break easily.

3.1. A/D CONVERTER AND DATA ACQUISITION SYSTEM.

UFT thermometers are characterized by a very good frequency response, (Haman et al., 1997, Rosa et al., 2005) which requires sampling frequencies exceeding 10000 samples per second. Available research aircrafts are not equipped in data acquisition systems (DAS) ensuring proper recording of UFT signals. Experience with commercially available data acquisition systems onboard research aircraft is that the records were affected by electromagnetic noise from radio, radar and avionic systems (Kumala et al., 2010). A new, dedicated compact DAS was designed and manufactured in order to complete construction of the UFT-2.

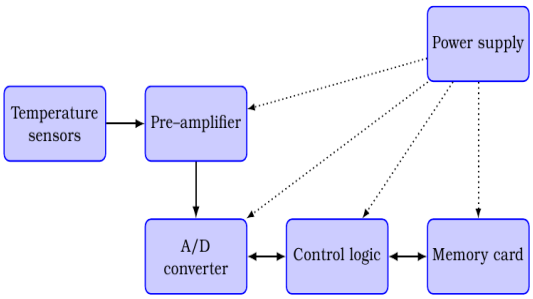

***Fig.3.** Block diagram of the complete UFT-2: sensing elements, amplifiers and data acquisition system (DAS).*

The dedicated UFT-2 DAS is completely autonomous and records signals on a static memory card. Signals are measured with MAX1167, low noise 16-bit A/D converter. MAX1167 output results in continuous data stream at rate up to 4.8 Mbps. Proper reception of such data stream requires

appropriate hardware. Therefore AT91SAM7S256, 32 bit micro-controller with ARM7 core was chosen.

Except for CPU and memories which are common in this class of devices, AT91SAM7S256 contains few additional hardware units. Two fast serial transmitters (SPI, SSC) and direct memory access unit (DMA) were used to transfer data between ADC and memory card. PWM unit was used to generate control signals for ADC. Due to utilization of these hardware blocks AT91SAM7S25 processing power was enough to control device. Block diagram of the firmware of the UFT-2 DAS is shown in Fig. 4.

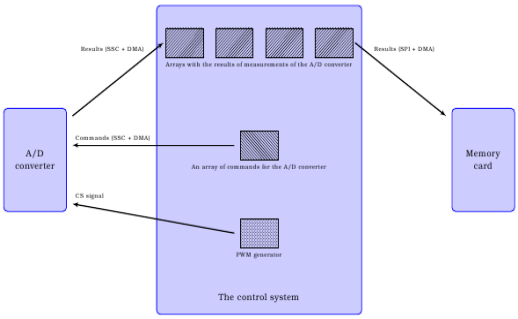

Fig.4. *Logic diagram of the UFT-2 DAS*.

DAS firmware is responsible for the initialization of the hardware subsystems and saving read data to the memory card. A/D converter uses two sets of arrays in RAM.

1. A single array store the configuration of individual measurements. The contents of the array is filled by software. Thus one have possibility to set customized configuration (the number of channels, sequence of measurements) by modifying the firmware.

2. Four arrays store results of measurements. Results are written periodically to the subsequent arrays with use of DMA unit. Set of arrays works as buffer and ensures enough time to rewrite these data to memory card.

The measurement results are finally stored on the MMC memory card. Maximum capacity of the card is 4 GB and provides nearly four hours of data recording at a speed of 100,000 measurements/sec. MMC memory card is controlled by the micro-controller using SPI unit.

A series of laboratory tests aimed at the verification of the performance of UFT-2 DAS were performed. A special effort was made to ensure that there is no signal leakage, no critical system failure or that no data is lost.

Laboratory-confirmed technical specification of the system is:

- maximum total sampling frequency 200 kS/s,
- four channels with sampling frequency up to 50kS/s per channel,
- resolution: 0.075mV (3mK),
- recording on MMC card of 4GB capacity.

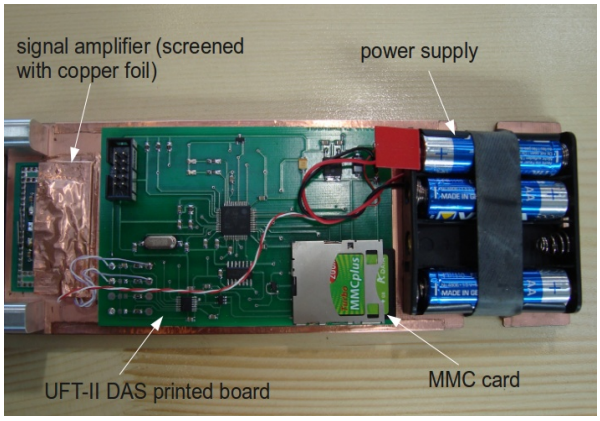

Fig.5. *UFT-2 electronics.*

A complete electronics of the prototype UFT-2 is shown in Fig.5.

4. TESTS IN FLIGHT.

Field tests of the UFT-2 with the dedicated DAS were performed in course of EUFAR-DENCHAR field campaign with the Enviscope Learjet aircraft, on 23/05–1/06 2011, in Höhn, Germany. Enviscope designed and built dedicated UFT-2 housing, capable to hold two UFT-II senors, amplifiers and the dedicated DAS (Fig.6.). It was mounted outside the measurement container under the right wing of the Learjet aircraft. (Fig.7).

In course of flight campaign one of ultrafine (1.25μm thick) wires was substituted by a resistor (fake sensor) in order to test amplifiers and data acquisition system.

The amplifiers and data acquisition system worked flawlessly in all research flights from the boundary layer up to stratosphere. In contrary, ultra-fine wires occurred delicate and broke in course of flights on this fast jet aircraft. Additional improvements are necessary in order to make the sensor robust, additional flight tests with thin film coated fiberglass sensors are necessary.

Nevertheless, enough data to characterize basic sensor performance was collected.

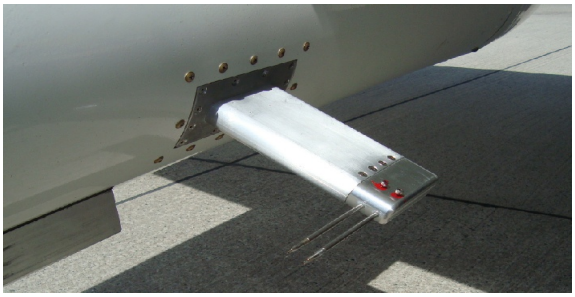

Fig.6. *Two UFT-II thermometers with housing designed and built by Enviscope in course of DENCHAR field intercomparison campaign.*

Fig.7. *UFT-2 in housing attached to the container under the left wing of Learjet aircraft.*

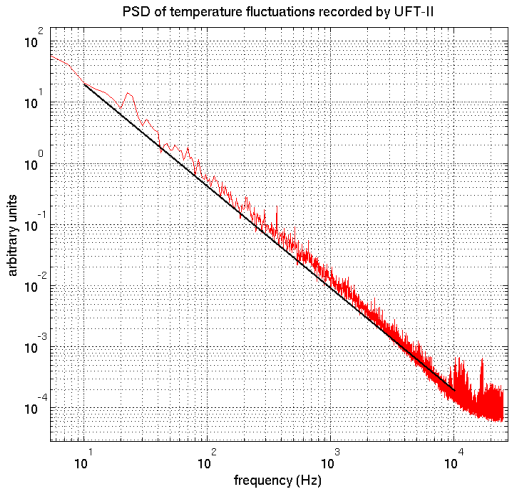

Fig.8. *Power spectral density of temperature fluctuations recorded with the UFT-2.*

In Fig. 8 power spectral density of temperature fluctuations in the atmospheric boundary layer recorded in a first phase of one of research flights. It can be seen that the record is free from the aerodynamic noise resulting from vortex shedding to frequencies up to 10 kHz. The relative amplitude of the noise is substantially smaller compared to the UFT-F sensors (c.f. Fig. 4 in Kumala 2010). Also, practically no signal damping (drop below -5/3 line) can be noticed for frequencies as high as 5kHz.

5. NUMERICAL TESTS

A large number of numerical experiments was performed in order to characterize flow around UFT-2. Transient direct numerical simulations were performed with the OpenFOAM® (Weller et al., 1998) code. The initially uniform, structured, hexagonal mesh was refined and deformed in such a way that it fitted a digital model of the UFT-2 geometry. In the region behind the rod cells had size between $(0.0012\text{mm})^3$ and $(0.05\text{mm})^3$. In some simulations the mesh with increased resolution was used in order to examine mesh-sensitivity of the results.

The numerical model solved incompressible Navier-Stokes equations using the PISO algorithm implemented in the so-called pisoFOAM solver. The equations were discretized using the finite volume method with the second order accuracy. The second order accurate Crank-Nicolson scheme was used to perform stable integration in the time domain. The time step used in most cases was equal to 4e-7s which resulted in the maximal value of the Courant number slightly below 3. The length of the time step was the main factor which influenced the large amount of computational time required by the simulations.

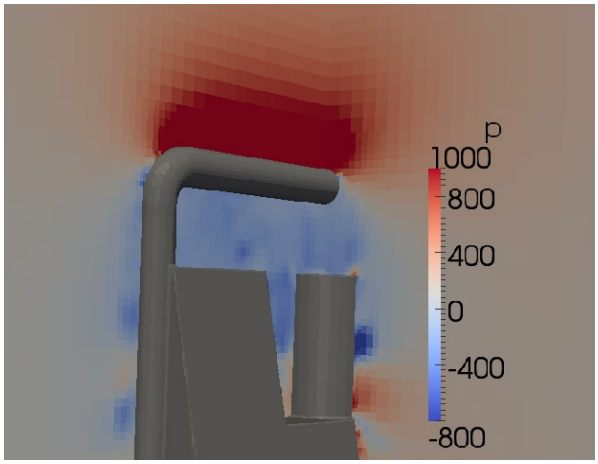

Fig.9. *A snapshot of pressure fluctuations behind the sensing rod at TAS 70m/s. Value of the pressure is given in Pascals divided by the air density.*

In all simulations uniform velocity of 70m/s was used as a inlet boundary condition along with a no-slip boundary condition at the surface of the thermometer.

Exemplary results of simulations are illustrated in Figs 9-13. In all the figures

sensor location is not shown (the sensor spanned the region between the middle cylinder and the sides, see Fig. 1).

Fig. 9 shows that the sensor is located in the area of slightly reduced pressure behind the rod.

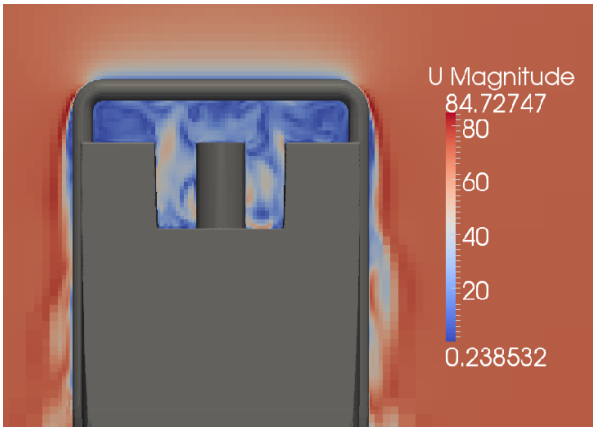

Fig.10. *A snapshot of air velocity magnitude in the plane of symmetry.*

Fig. 10. presents magnitude of air velocity around the senor. It can be seen, that in the position of sensing element velocity is reduced from 70m/s TAS down to 30-50m/s.

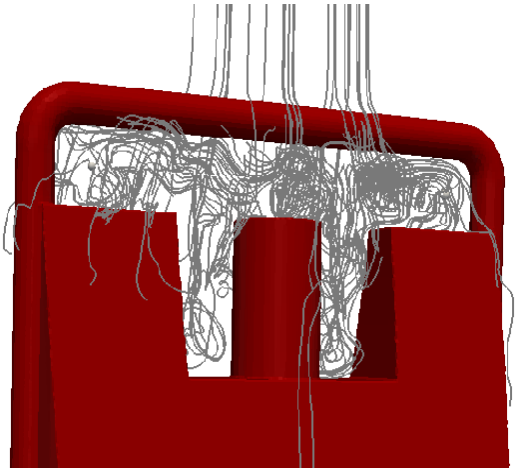

Fig.11. *Streamlines indicating recirculation of the flow behind the rod and escaping after recirculation. Air represented by these streamlines gets to the measurement volume – location of the sensing element*

Figs 11 and 12 show streamlines: few of them are trapped in a wake of the rod, and escape the wake after some recirculations (Fig. 11), while most of them flow around the sensor head. (Fig.12).

Reduction of velocity behind the rod and some recirculation should effect in reduction of the frequency response of the senor. This effect is shown in Fig.13, in which simulation of a sharp front of passive scalar advected with a flow is simulated and response of a modeled sensing element is investigated.

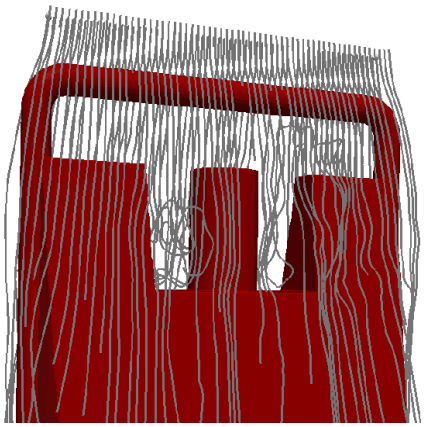

Fig.12*. Streamlines indicating airflow around the senor head. Air represented by these streamlines cannot be in contact with the sensing element.*

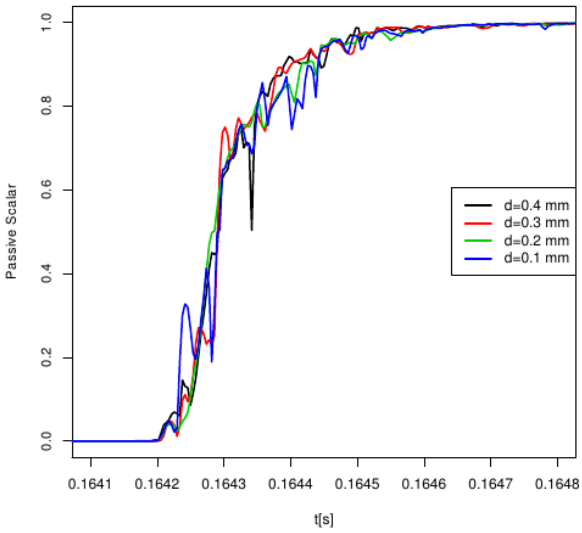

Fig.13. *Response of the "synthetic" sensing element placed 0.75mm behind the protecting rod to the step-like passive scalar (e.g. temperature) jump in the flow.*

Presented curves refer to value of the passive scalar collected from four points uniformly distributed along the sensing element. It is shown, that the disturbance of the flow and some recirculation behind the rod slightly reduce frequency response of the senor. In effect after 0.0002s sensing element can recover about 80% of initial passive scalar jump. The same simulation was performed with the mesh resolution twice as large as for results presented above, showing almost the same response of the sensing element.

The estimated response time better than 0.0002s is in agreement with the PSD of temperature fluctuation shown in Fig. 8,

where some damping of frequencies above 5kHz can be noticed.

Acknowledgments:

This research was funded as a part of Joint Research Activity JRA-1 in frames of the EUFAR EU FP-7 project nr 227159 supported by Polish Ministry Of Science matching fund 1283/7. PR UE/2010/7.

References:

Haman, K.E., A. Makulski, S. P. Malinowski, and R. Busen, 1997: A new ultrafast thermometer for aiborne measurements in clouds. *J. Atmos. Oceanic Technol.*, **14**, 217–227.

Haman, K.E., S.P. Malinowski, B.D. Struś, R. Busen and A. Stefko, 2001: Two new types of ultrafast aircraft thermometers, *J. Atmos. Ocean. Technol.*, **18**, 117-134.

Kumala, W., K. E. Haman, M. Kopec, and S. P. Malinowski, 2010: Ultrafast thermometer UFT-M and high resoltution temperature measurements in Physics of Stratocumulus Top (POST). 13th AMS Conference on Cloud Physics 28 June–2 July 2010, Portland, OR USA, http://ams.confex.com/ams/pdfpapers/170832.pdf

Rosa B., Bajer K.; Haman K.E.; Szoplik T., 2005: Theoretical and experimental characterization of the ultrafast aircraft thermometer: Reduction of aerodynamic disturbances and signal processing. *J. Atmos. Ocean. Technol.*, **22**, 988-1003.

Weller H. G., Tabor G., Jasak H., Fureby C., 1998: A tensorial approach to computational continuum mechanics using object-oriented techniques. *Computers in Physics* **12**, 620–631